Electrophoresis of end-labeled DNA: Theory and experiment

Henry W. Lau and Lynden A. Archer*
School of Chemical and Biomolecular Engineering, Ithaca, New York 14853, USA
(Received 20 August 2009; revised manuscript received 28 January 2010; published 25 March 2010)

The dynamic behavior of end-labeled DNA during free-solution electrophoresis is investigated using a simple dumbbell model for the labeled DNA. We study the effect of the applied field, label size, and chain stiffness on DNA conformation and electrophoretic mobility. High applied fields are predicted to magnify the size-dependence of mobility and to yield a nonmonotonic dependence of electrophoretic mobility on applied field. The effectiveness of leveraging label size and DNA chain stiffness for improving resolution is also discussed in the context of DNA deformation. To evaluate the most salient model predictions, we use capillary electrophoresis experiments to characterize the size- and field-dependent mobility of dsDNA fragments (300 bp–2 kbp) end-functionalized with streptavidin. Our experimental results are found to be in generally good accord with expectations based on the dumb-bell model. We discuss implications of these findings for fast, size-based separation of DNA in free solution.

DOI: 10.1103/PhysRevE.81.031918 PACS number(s): 87.15.Tt

I. INTRODUCTION

Size-based separation of DNA fragments has been a key enabler for progress in areas such as genomic sequencing, mutation detection, and forensics. Historically, the size independent free-solution mobility of DNA molecules above a certain critical size (approximately 400 bp for dsDNA, with most changes in mobility occurring below 110 bp [1], and 10 bases for ssDNA [2,3]) has necessitated the use of sieving media to achieve separation via electrophoresis. By end-labeling DNA molecules with a uniform, neutral drag-inducing body or tag, it is now widely recognized that size-based separation can be achieved even in the absence of a sieving medium. Termed end-labeled free-solution electrophoresis (ELFSE) [4], this method has the potential to dramatically expedite the fractionation process by allowing the elimination of the sieving matrix.

The works of Long *et al.* on the electrophoresis of polyampholytes have served as a key framework for analyzing mobility of end-labeled nucleic acids [5,6]. For a Gaussian chain composed of sections that differ in charge, the net electrophoretic mobility is computed as the average mobility of the individual monomers. Because this formulation assumes that the charged and uncharged monomers do not differ in size, the theory can only be employed for DNA-protein conjugates if the disparate hydrodynamic properties of their monomers are explicitly taken into account. Initially, "blob" models were used to group DNA monomers into subsections, or blobs, of hydrodynamic radii equal to the radius of the spherical label [7]. Subsequent efforts to study conjugates containing flexible polymeric labels divide both the charged and neutral segments of the chain into blobs. The mobility of such molecules, can be expressed in terms of the number of monomers N_i in each segment ($i=1$ for DNA; 2 for the neutral label) and the free-solution mobility μ_0 of the DNA,

$$\mu = \frac{N_1}{N_1 + \alpha}\mu_0, \tag{1}$$

Here, $\alpha=\alpha_2 N_2$ is the number of charged monomers that is hydrodynamically equivalent to the entire neutral label, with the factor $\alpha_1=(b_2 b_{k,2})/(b_1 b_{k,1})$ depending on both the monomer size b_i and the Kuhn step length $b_{k,i}$ of each component. Equation (1) can be used to describe the electrophoretic motion of end-labeled DNA as long as both components remain in their equilibrium conformation. In response to the application of a sufficiently large electric field, conjugates can in fact assume a segregated conformation (i.e., the charged segment becomes disentangled from the neutral label). Alternatively, steric segregation may occur if the label size greatly exceeds the persistence length of the DNA, thus preventing it from wrapping around the label [7]. For these cases, the mobility can be shown to be of the form [5,8]

$$\mu = \frac{\zeta_1}{\zeta_1 + \zeta_2}\mu_0, \tag{2}$$

where ζ_1 and ζ_2 are the friction coefficients of the DNA and label, respectively. In using Eq. (2) to predict the mobility of a segregated conjugate, it is clear that the friction of both sections must be correctly evaluated. This in turn requires detailed knowledge of the characteristic size and conformation of both the DNA and the neutral label under the electrophoresis running conditions.

Results from numerous ELSFE experiments have been successfully analyzed using Eq. (1) [9], indicating that the DNA and the label remain randomly coupled under typical conditions. Indeed, simulation results have shown that the field values in past studies are too low to induce hydrodynamic segregation of ssDNA from the end label [10]. With the critical field required for such deformation (>1 kV/cm) exceeding the capacity of most current CE setups [11], experimental observation of the segregated regime, under which Eq. (2) would apply, remains lacking. The seminal work by Heller *et al.*, which reported the fractionation of streptavidin-labeled dsDNA fragments, provided key valida-

*laa25@cornell.edu

tion of ELFSE as a separation technique [12]. With the radius of the streptavidin label R_{Stv} (~2.7 nm) [13] being much smaller than the Kuhn length of dsDNA (~100 nm), dsDNA molecules of no more than $3b_k$ (~900 bp) are evidently too short to maintain a random walk conformation around the attached protein. Instead they are thought to assume sterically segregated structures for which Eq. (1) applies. Although the authors discussed the likely segregated nature of the streptavidin-labeled dsDNA, they based their conclusion on the fact that their experimental data, when presented as a plot of $\mu_0/\mu-1$ versus N_1^{-1} (or M^{-1} in their nomenclature), exhibits a linear regime {see inset of Fig. 1(a) in Ref. [12]}. In actuality, it is for *unsegregated* conjugates that such a presentation of mobility values is expected to manifest a linear dependence on N_1^{-1} [see Eq. (1)]. For conjugates whose components are hydrodynamically distinct, and with a charged section represented as a cylinder of random orientation, Eq. (2) indicates that $\mu_0/\mu-1$ scales linearly with $N_1^{-1}\ln(N_1)$ and is concave when plotted against N_1^{-1}. In other words, it is a plot of $[\mu_0/\mu-1]/\ln(N_1)$ vs. N_1^{-1} that should yield a straight line. In the aforementioned figure of Heller *et al.*, the paucity of data points for long DNA fragments makes it difficult to discern unambiguously the trend for small N_1^{-1}.

Recent theoretical studies focusing on ELFSE at high fields have predicted substantial improvements in read length for conjugates whose constituents are segregated and completely stretched [14]. In the high field regime, it is apparent that the interplay between the electric field, which stretches the chain, and the intrinsic DNA stiffness, which acts to maintain the equilibrium conformation, plays an important role in setting the dynamics of the conjugates. In light of practical limitations on inducing hydrodynamic segregation via the applied field, sterically segregated streptavidin-dsDNA complexes stand as an attractive model system to assess theoretical predictions for the dynamics of end-labeled DNA at currently inaccessible field intensities.

In the present work we study free-solution electrophoresis of hydrodynamically segregated DNA-protein conjugates with the help of a simple elastic dumbbell model. Because our analysis takes into account the elasticity of the deformed DNA fragment, it provides a more accurate assessment of the forces on the tag, as well as of the overall DNA-size-dependence of the electrophoretic mobility of conjugates. To determine the range of validity of mobility values predicted using this model, we perform CE studies of dsDNA-streptavidin complexes in Tris-TAPS-EDTA. Streptavidin remains uncharged under the running conditions used for the study, which makes the hydrodynamically segregated DNA-tag construction uniformly applicable over the range of fields studied.

II. MATERIAL AND METHODS

Double-stranded DNA (dsDNA) fragments ranging in size from 375 bp to 3.5 kbp were synthesized via PCR with M13mp18 single-stranded viral DNA (NEB, Ipswich, MA, USA) serving as template. The biotinylated, FITC-labeled forward primer as well as the reverse primers were obtained from Sigma (Woodlands, TX, USA). Amplification of the template was carried out using an MJ Research PTC-200 Alpha thermal cycler and 40 cycles of denaturation (95 °C, 50 s), annealing (50 °C, 60 s), and extension (72 °C, 60 s). The reaction mixture for each fragment size consisted of 5 ng template, 0.5 μM of forward and reverse primers, 250 μM of each nucleotide (dATP, dTTP, dCTP, dGTP), and 1 unit of Taq polymerase in a total volume of 50 μl. The PCR products were purified via agarose gel electrophoresis [1% agarose in 1X tris-acetate-EDTA (TAE) buffer], extracted using a commercial gel extraction kit (QIAGEN, Valencia, CA, USA), and suspended in 10 mM Tris-Cl, *p*H 8.5. Stock solutions of protein label was made using streptavidin (Sigma) suspended in phosphate buffered saline *p*H=7.2 (Sigma). The concentration of the protein solution and the purified DNA fragments was determined using a SmartSpec 3000 spectrophotometer (Bio-rad, Hercules, CA) via absorbance measurements at 280 and 260 nm, respectively. The extinction coefficient $\varepsilon_{280\ \mathrm{nm}}^{0.1\%}$ for streptavidin was taken to be 3.4 [15].

Streptavidin stock solution was mixed with PCR products at appropriate volumes to ensure a 20:1 molar ratio of protein to DNA, in order to minimize the conjugation of more than 1 biotinylated DNA molecule to the four binding sites present on the protein. The mixture was incubated at 28 °C for 30 min and stored at 5 °C. Immediately before electrophoresis, the streptavidin-DNA mixture was diluted by five times the volume of the running buffer. Identical dilution and mixing steps were performed for the unlabeled DNA samples in the absence of the protein label.

Capillary electrophoresis measurements were performed on a GPA100 capillary electrophoresis unit (Groton Biosystems, Boxborough, MA), fitted with a 75 μm internal diameter fused silica capillaries (Polymicro Technologies, Phoenix, AZ) filled with 1x Tris-TAPS-EDTA (TTE) (Sigma, St. Louis, MO) with 1% POP-6 (v/v) (Applied Biosystems, Foster City, CA). Capillaries were rinsed with 1M HCl (30 min), DI H_2O (30 min), 1M NaOH (30 min), and DI H_2O (30 min) before running buffer is introduced. The capillary was flushed with running buffer at 1500 bar (2 min) before each measurement commenced. Samples were loaded by pressure injection at 200 bar for 0.2 s. The fluorescence intensity at a detection window 29.9 cm from the inlet was recorded using a laser induced fluorescence detector (Picometrics, Ramonville, France). 30, 15, and 5 kV were applied to capillary of overall length 77.8 cm, corresponding to field strengths of 386, 193, and 64.3 V/cm, respectively. Despite the inclusion of POP to suppress EOF, residual electro-osmotic flow μ_{eof} within the fused silica capillary was measured according to the protocol in [16] with Coumarin 334 (Sigma, St. Louis, MO) as the neutral marker. The effective mobility μ is thus calculated from the observed mobility μ_{obs} according to

$$\mu = \mu_{obs} - \mu_{eof}. \tag{3}$$

III. RESULTS AND DISCUSSION

Figure 1(a) shows the mobility of labeled and unlabeled dsDNA. Whereas the mobility values of the unlabeled DNA

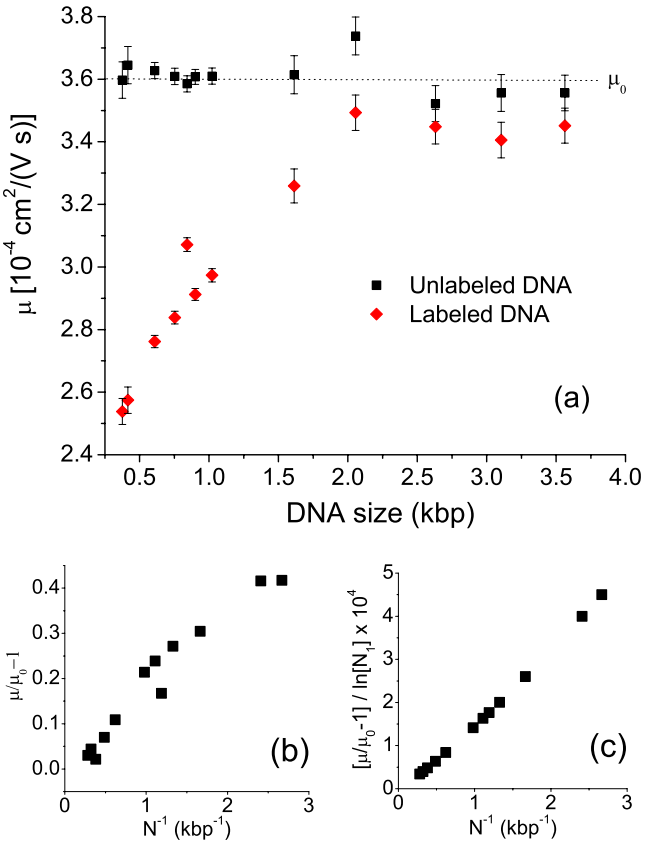

FIG. 1. (Color online) (a) Mobility μ plotted against size of unlabeled and labeled DNA. (b) $\mu_0/\mu-1$ plotted as a function of N_1^{-1}. (c) $[\mu_0/\mu-1]/\ln(N_1)$ plotted as a function of N_1^{-1}.

are scattered around an average of 3.61×10^{-4} cm^2/(V s), the mobility of the conjugates is characterized by two regions of behavior. Beyond 2 kbp, a plateau region is noted where the mobility of the conjugate approaches that of the unlabeled DNA as the relative size of the charged segment renders negligible the effects of protein end-labeling on the overall motion of the conjugate. For DNA sizes under 1.5 kbp, the presence of the label leads to a size-dependent mobility that allows separation. In order to determine if the constituents of the labeled molecules are hydrodynamically distinct, their mobility values are first plotted as $\mu_0/\mu-1$ versus N_1^{-1}. At low values of N_1^{-1}, deviations from linearity can be noted in Fig. 1(b), where a larger slope can be observed for larger DNA. This contrasts with the plot of $[\mu_0/\mu-1]/\ln(N_1)$ vs. N_1^{-1} in Fig. 1(c), where the data set shows an unambiguous linear trend that is maintained throughout the entire size range. Thus, it appears that dsDNA is indeed sterically segregated from the streptavidin label and that the electrophoretic mobility of this particular conjugate system can be described using Eq. (2).

Although the correct trend is obtained, a weakness in the above approach lies in the implicit assumption that the DNA has already taken on a fully extended conformation. A more rigorous analysis would instead model the charged segment as a cylinder with length equal to the field-dependent end-to-end distance of the DNA.

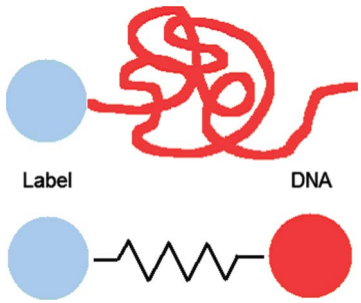

FIG. 2. (Color online) Representation of hydrodynamically segregated DNA-protein conjugate as elastic dumbbell.

A. Model development

We model an end-labeled DNA as a pair of friction spheres (one representing the protein label and the other the polyelectrolyte), connected by an elastic spring of length equal to the end-to-end distance of the DNA (Fig. 2). The probability density $\psi(t,\bar{R};E)$ of finding a spring with connector vector $\bar{R}$ is [17]

$$\frac{\partial\psi}{\partial t}=-\bar{\nabla}\cdot\left\{[\bar{\bar{\kappa}}\cdot\bar{R}]\psi-kT\left(\frac{1}{\zeta_1}+\frac{1}{\zeta_2}\right)\bar{\nabla}\psi-\left(\frac{1}{\zeta_1}+\frac{1}{\zeta_2}\right)\bar{F}^C\psi+\frac{\bar{F}_2^E}{\zeta_2}\psi-\frac{\bar{F}_1^E}{\zeta_1}\psi\right\},\tag{4}$$

where subscripts $i=1,2$ refer to the DNA and the label, respectively. For bead i, ζ_i gives its friction coefficient and $\bar{F}_i^E$ represents the electric force acting on it. $\bar{F}^C$ is the connector spring force. We limit Eq. (4) to near-neutral charge of protein drag tag candidates ($\bar{F}_2^E=0$), and to situations where bulk electro-osmotic flow is suppressed, as in typical CE experiments ($\bar{\bar{\kappa}}=0$). The electric force acting on bead 1 during electrophoresis can be readily computed as $\bar{F}_1^E=v_{el}\zeta_1=\mu_{0,1}\bar{E}\zeta_1$. Substituting these results in Eq. (4) we find at steady-state

$$0=\bar{\nabla}\psi-\frac{1}{kT}\left[\mu_{0,1}\bar{E}\left(\frac{\zeta_1\zeta_2}{\zeta_1+\zeta_2}\right)-\bar{F}^C\right]\psi=\bar{\nabla}\psi-\frac{\partial\lambda}{\partial\bar{R}}\psi,\tag{5}$$

with λ defined as

$$\lambda\equiv\frac{1}{kT}\left\{\left[\zeta_2\mu_{0,1}\int\frac{\zeta_1}{(\zeta_1+\zeta_2)}\bar{E}\cdot d\bar{R}\right]-\left[\int\bar{F}^C\cdot d\bar{R}\right]\right\}.\tag{6}$$

To compute the spring force, we employ the Marko-Siggia interpolation expression for wormlike chains [18]; it is understood that predictions based on this model are exact only in the long chain limit. The unknown drag coefficient ζ_2 in Eqs. (5) and (6) is then estimated using Stokes' law by approximating the label as a rigid sphere.

The field-induced friction originating from the motion of the counterions is already accounted for implicitly by $\mu_{0,1}$, which means that the friction coefficient ζ_1 is strictly of hydrodynamic origin and, as such, depends on the DNA con-

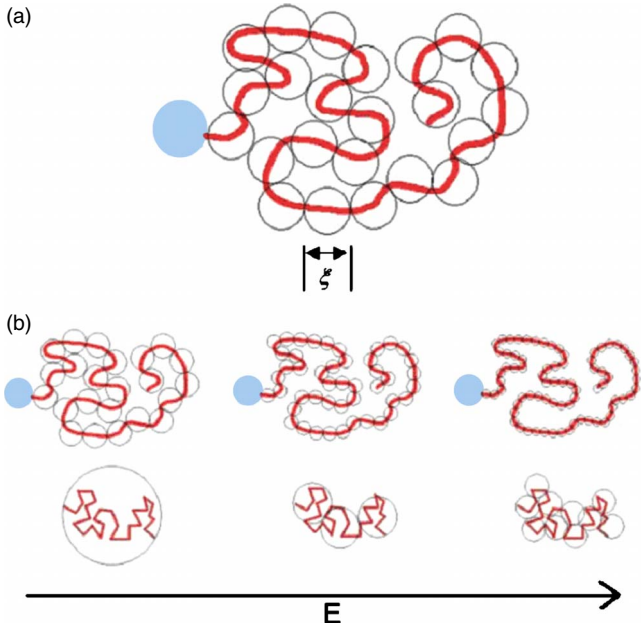

FIG. 3. (Color online) (a) Division of DNA into blobs of electrical energy O(kT). (b) Representation of the expected decrease in blob size (i.e., decrease in number of Kuhn steps per blob) and increase in number of blobs at increasing applied field.

formation and applied field. Specifically, alignment of DNA segments at progressively higher applied fields renders ζ_1 anisotropic and changes the qualitative relationship between ζ_1 and DNA fragment size. To determine $\zeta_1(E,R)$, we employ a blob model for the DNA [19], in which the polyelectrolyte chain is divided into N_b identical subsections, or blobs, each of size ξ and electrical energy kT [Fig. 3(a)]. Setting $F_1^E \approx kT/\xi$ for a section of size ξ yields

$$kT \approx \mu_0 E \zeta_b \xi. \tag{7}$$

The friction per blob ζ_b depends on the number of Kuhn steps g within the section and the friction of a single Kuhn segment ζ_k,

$$\zeta_b = g\zeta_k. \tag{8}$$

On length scales smaller than ξ, the chain is unperturbed by the electric field and obeys ideal chain statistics, $\xi^2 \approx g b_k^2$. Rearranging to solve for g and substituting into Eqs. (7) and (8) yields,

$$\xi \approx \left[\frac{kTb_k^2}{\mu_0 E \zeta_k}\right]^{1/3}. \tag{9}$$

Thus, as the applied field is increased, the blob size reduces [Fig. 3(b)] until it becomes comparable to the Kuhn steplength b_k, and the DNA can be modeled as an oriented stick of length $R=R_{\max} \approx N_k b_k$. Under the influence of more moderate electric fields, blobs will align to form cylindrical, rodlike structures of end-to-end length $R \approx N_b \xi$. The friction of a DNA chain comprising of N_b sections is then given by $\zeta_1 \approx N_b \zeta_b$, which can be rewritten using Eqs. (8) and (9) as

$$\zeta_1 \approx R\left[\frac{kT}{\mu_0 E}\right]^{1/3}\left[\frac{\zeta_k}{b_k^2}\right]^{2/3}. \tag{10}$$

The friction of a single Kuhn step is taken to be that of a cylinder of length b_k and diameter d oriented randomly with respect to the direction of electrophoretic motion,

$$\zeta_k = \left[\frac{10}{3}\right]\pi\eta b_k \ln\left[\frac{b_k}{d}\right]^{-1} \tag{11}$$

Since Eq. (10) is only valid as long as random walk statistics are obeyed by segments within the blob, an alternate description for DNA friction must apply for $\xi \leq b_k$. The critical electric field E^* corresponding to $\xi \approx b_k$ can be found by setting Eq. (9) to b_k,

$$E^* \approx \frac{kT}{\mu_0 \zeta_k b_k}. \tag{12}$$

Physically, E^* marks the field above which the friction experienced by the charged chain becomes equivalent to the sum of the friction experienced by all Kuhn segments in isolation. This corresponds to the situation where there is significant stretching of the chain, with the Kuhn segments becoming mostly aligned in the direction of the electric field. The friction that corresponds to an elongated chain of N_k Kuhn steps and end-to-end distance $R \approx N_k b_k$ is

$$\zeta_1 \approx N_k \zeta_k \approx 2\pi\eta \ln\left[\frac{b_k}{d}\right]^{-1} R, \tag{13}$$

where the numerical prefactor reflects the essentially parallel orientation of the Kuhn segments relative to the direction of motion.

To construct theoretical mobility curves, the appropriate expression for DNA friction [i.e., either Eqs. (10) or (13), dictated by the applied field relative to E^*] is substituted into Eq. (5), which is then numerically integrated. The solution to Eq. (5), which gives the distribution function, is found by $\psi = \exp[\lambda]$, thus allowing the equilibrium end-to-end distance to be computed via

$$R = \frac{\int_0^{2\pi} d\phi \int_0^{\pi} \sin\theta d\theta \int_0^{\infty} R\psi R^2 dR}{\int_0^{2\pi} d\phi \int_0^{\pi} \sin\theta d\theta \int_0^{\infty} \psi R^2 dR}. \tag{14}$$

The value of R for DNA of varied sizes and applied field is used to obtain the reduced mobility via Eq. (2).

B. Model validation

In order to use this model to predict mobilities obtained from experiment, an appropriate description of DNA friction [i.e., either Eq. (10) or (13)] is needed. As discussed above, Eq. (12) provides an estimate for the critical electric field at which the charged chain becomes significantly stretched. While $E^* \approx 4.3$ kV/cm for ssDNA, E^* for dsDNA conjugates is approximately 43 V/cm, implying that under field values applied in this work (as well as in typical CE experiments), the relative mobility should be given by a combination of Eqs. (2) and (13),

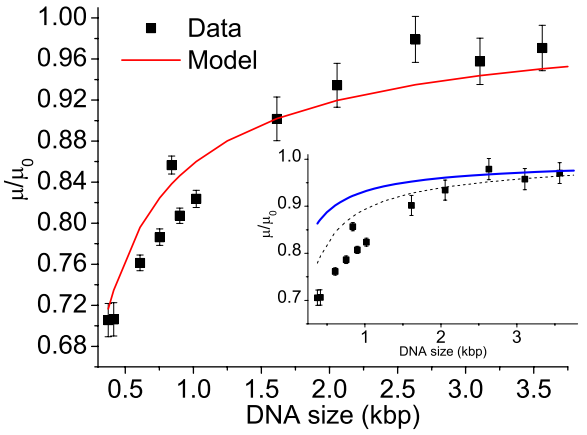

FIG. 4. (Color online) Reduced mobility plotted against DNA size, with theoretical curve constructed via Eq. (15). Inset shows predictions made by describing DNA friction using Eq. (10) (lower, broken curve) and by treating DNA as rigid cylinder of contour length $N_1 b_1$ (upper, solid curve).

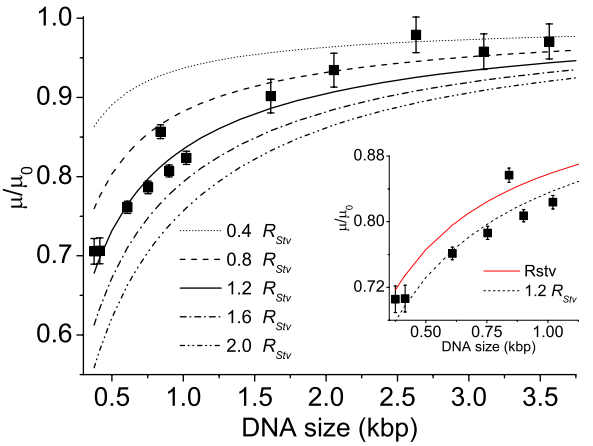

FIG. 5. (Color online) Reduced mobility plotted against DNA size, with theoretical curves constructed using label radii ranging from 0.4 R_{Stv} to 2.0 R_{Stv} Inset shows predictions made by setting label radius to R_{Stv} (upper, solid curve) and 1.2 R_{Stv} (lower, dotted curve).

$$\mu_r = \frac{\mu}{\mu_0} = \frac{\zeta_1}{\zeta_2 + \zeta_1} \approx \frac{R}{3R_{Stv} \ln\left[\frac{b_k}{d}\right] + R} \tag{15}$$

with R_{Stv} being the radius of the streptavidin label and $\zeta_2 = 6\pi\eta R_{Stv}$.

In Fig. 4, the relative mobility as computed from the measured mobility of both labeled and unlabeled DNA is presented as a function of DNA size. Using only physical properties (e.g., b_k and d for dsDNA, R_{Stv} for the label, η for solvent), experimentally imposed values (e.g., E, DNA sizes), and an average, measured value for μ_0 [from Fig. 1(a)], the relative mobility can be readily calculated via Eq. (15). The resulting theoretical curve matches the experimental data remarkably well, providing reasonable predictions for both the size dependence and the actual values for μ_r. The importance of selecting the correct friction expression for the labeled DNA is underscored by the discrepancy between predictions based on Eq. (10) and experimental data for DNA sizes less than 1.5 kbp (Fig. 4 inset). Also apparent is the fact that complete stretching of the DNA to its contour length cannot be assumed, as the corresponding theoretical curve compares even more poorly with data.

Within the region of high resolution (i.e., for DNA less than 1 kbp), the positive deviations of model predictions from data can be attributed to an apparent underestimation of the drag imposed by the label. Whereas prior crystallographic study of streptavidin has shown that each of the tetrameric protein's four monomers come together to yield an oblonged structure [13], the label was modeled as a sphere in order to permit the use of Stoke's expression to calculate protein drag. The effective radius R_{Stv} of the protein label was taken to be the average half-width of streptavidin (2.7 nm), as calculated from its crystal dimensions. Thus, the overprediction of μ_r suggests that the approximated value for R_{Stv} is actually smaller than the hydrodynamic or Stoke's radius of streptavidin, causing the label drag to be underestimated. This effect diminishes when the hydrodynamic drag of the charged chains becomes dominant, leading to improved fit between predictions and data for larger DNA. By treating the label radius as a free parameter, an estimate for the "actual" Stoke's radius of streptavidin can be inferred from experimental data. In Fig. 5, theoretical curves constructed by varying the label radius are presented along with measurements. It can be observed that by taking the radius to be 20% larger than R_{Stv}, corresponding to a value of ~3.2 nm, the model provides a superior description of μ_r within the region of high resolution (Fig. 5 inset). For longer DNA, the use of this larger radius value leaves mostly unchanged the fit quality between theory and data.

For $E > E^*$, the relative mobility as given by Eq. (15) lacks an explicit dependence on the magnitude of the applied field, suggesting that the application of varied field strengths within this regime should elicit only minor changes in mobility. Where there is change, the mobility for a given conjugate is anticipated to be larger at higher fields, due to field-induced stretching and/or alignment of the charged section. Consistent with intuition, μ_r measured at three different applied fields reveal only a weak dependence on E, with the maximum mobility change being no more than 5% across the field strengths studied (Fig. 6). In general, the intrinsic stiffness of double-stranded DNA molecules imposes a high force requirement for chain extension, thus limiting the effect of the applied field on mobility. By contrast, the greater flexibility of their single-stranded counterpart suggests that the dynamic behavior of end-labeled ssDNA should display an enhanced sensitivity to factors that affect their end-to-end size. To further explore how chain conformation affects the motion of conjugates whose charged component is highly flexible, our model is extended to describe the electrophoresis of ssDNA-protein conjugates and to predict the influence of applied field, chain stiffness, and label size on their separation.

C. Model predictions for ssDNA

For hydrodynamically segregated ssDNA conjugate at fields $E < E^*$, the charged chain is expected to assume a

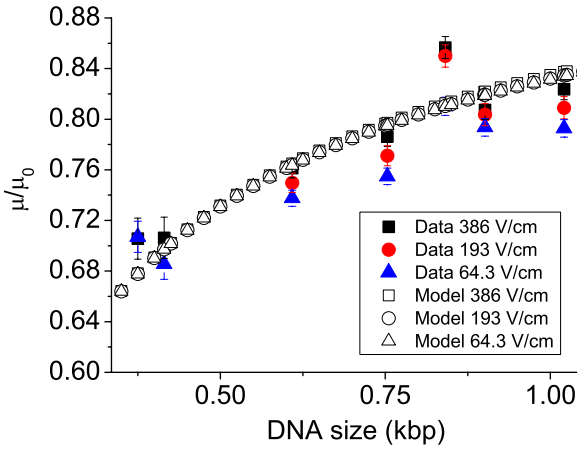

FIG. 6. (Color online) Reduced mobility plotted against DNA size for applied field strengths of 386, 193, and 64.3 V/cm. Corresponding model predictions (with label size set to 1.2 R_{Stv}) are also shown.

moderately stretched conformation. Unlike dsDNA, the Kuhn length of ssDNA is small enough to render experimentally relevant the regime in which Eq. (10) applies (i.e., for the operating electric field to be less than E^*). The associated expression for μ_r is

$$\mu_r = \frac{\mu}{\mu_0} = \frac{\zeta_1}{\zeta_2 + \zeta_1} \approx \frac{R}{6\pi\eta R_{Stv}\left[\frac{\mu_0 E}{kT}\right]^{1/3}\left[\frac{b_k^2}{\zeta_k}\right]^{2/3} + R}. \tag{16}$$

1. Influence of field

An increase in electric field is matched by an increase in the end-to-end distance of the charged chain, as shown in Fig. 7. A longer molecule, possessing a greater number of charges for the electric field to act upon, undergoes a higher percentage extension than a shorter molecule. This change in chain conformation magnifies the mobility difference among the conjugates, leading to enhanced separation (Fig. 8). Al-

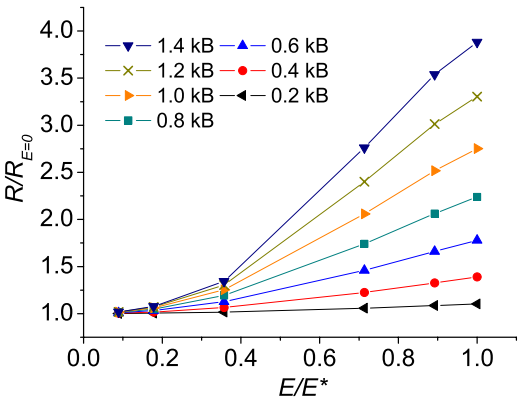

FIG. 7. (Color online) Plots of end-to-end distance R (normalized by equilibrium end-to-end distance at $E=0$) against applied field (normalized by critical field E^*) for DNA lengths ranging from 0.2 to 1.4 kilobases.

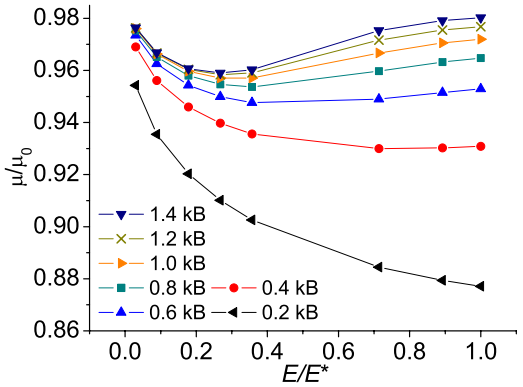

FIG. 8. (Color online) Plots of reduced mobility against applied field (normalized by critical field E^*).

though conjugates of longer DNA molecules are always predicted to elute sooner, the mobility of the conjugates do not depend monotonically on the applied field.

This result can be explained by recognizing that higher fields can bring forth effects that act to both promote and retard electrophoretic motion. Treating the electrophoretic velocity as a ratio of the electric force on the conjugate (which depends on conjugate charge q_1) and its friction coefficient yields

$$v_{el} = \frac{F_1^E}{\zeta_1(E)} = \frac{q_1 E}{\zeta_1(E)}, \tag{17}$$

where the change in $\mu \equiv v/E$ with respect to field can now be obtained as

$$\frac{\partial \mu}{\partial E} = -\frac{q_1}{\zeta_1(E)^2}\frac{\partial \zeta_1(E)}{\partial E} + \frac{q_1}{E\zeta_1(E)}. \tag{18}$$

Physically, an augmented field increases both the friction coefficient of the DNA (by elongating the charged chain) [i.e., $\partial\zeta_1(E)/\partial E > 0$] and the driving force for motion. Whereas the former effect acts to slow the molecule, the latter acts to accelerate it. Equation (18) embodies this competing effect with the presence of a negative first term, which has a stronger dependence on $\zeta_1(E)$ than the second, positive term. Because longer DNA correspond to larger values of $\zeta_1(E)$, their mobility values must begin to increase with field as $\zeta_1(E)$ becomes sufficiently large to render the first term of Eq. (18) negligible. For these molecules, Eq. (18) also calls for the slope of μ/μ_0 plotted against E (i.e., $\partial\mu/\partial E$) to diminish as their $\zeta_1(E)$ increases along with E. Both of these behaviors are observed in Fig. 8.

At fields above E^*, the almost rodlike conformation taken by the DNA forces the dynamics of the conjugates to subscribe to a different field dependence. Operating at this field regime is predicted to bring forth substantially enhanced resolution, with the greatest effect on the separation of smaller molecules (Fig. 9). Although subsequent increases in applied field appears to diminish the mobility differences between conjugates of varying sizes, the magnitude of the differences remains significantly greater than those predicted for $E < E^*$. Around $E = E^*$, a transition region exists in which some sections of the labeled DNA become strongly oriented by the

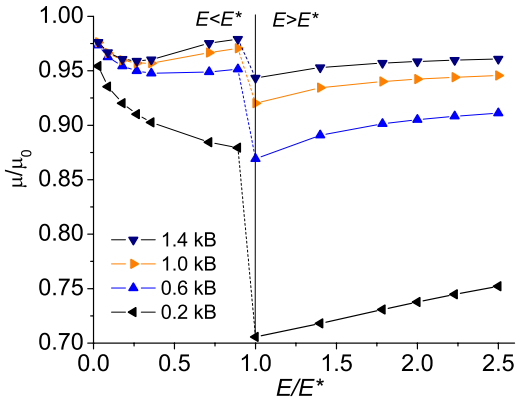

FIG. 9. (Color online) Plots of reduced mobility against applied field (normalized by critical field E^*) for ssDNA of lengths 0.2-, 0.6-, 1.0-, 1.4-kilobases. Vertical line at $E=E^*$ is included to guide the eyes.

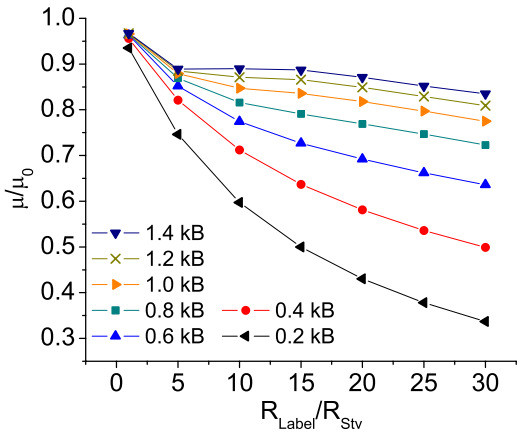

FIG. 11. (Color online) Plots of reduced mobility against label radius [normalized by streptavidin radius (2.7 nm)] for various DNA sizes.

field while other sections maintain their random orientation. Within this region, some combination of Eqs. (10) and (13) is required to properly describe the friction of the entire DNA chain.

2. Influence of label size

Besides the electric field, molecular deformation can be magnified by using labels with higher drag. For spherical labels, such as globular proteins or surfactant micelles [20,21], this corresponds to increases in the radius of the label. Physically, a larger drag tag generates more friction via its increased surface area and, in doing so, promotes the stretching of the attached DNA during electrophoresis. In Fig. 10, label size is shown to affect the equilibrium size of longer DNA more strongly, as these molecules exhibit a greater degree of deformation for larger labels. In terms of mobility, larger drag tags are more effective in retarding the motion of smaller DNA. This means that the mobility difference among shorter DNA must be more sensitive to label size than longer DNA (Fig. 11). Although the demand in maximizing read length appears to call for tags with ever greater drag, their use as labels is limited by the concomitant reduction in throughput caused by the resultant decrease in electrophoretic velocity.

3. Influence of chain stiffness

The sharp difference in the magnitude of E^* for ss- and dsDNA highlights the important role played by chain stiffness in setting the conformation and motion of end-labeled DNA. For polymer chains of identical contour length, higher local stiffness (i.e., longer Kuhn length) corresponds to greater equilibrium end-to-end distances. With the applied field kept constant, the conformation of end-labeled DNA can be made more elongated if the local stiffness were increased (Fig. 12). Experimentally, higher chain stiffness can be achieved through the use of low ionic strength running buffers. A decrease in the ionic strength from 10^{-1} to 10^{-3} has been reported to educe an increase in the Kuhn length of ssDNA by approximately fourfolds [22]. Such a change in the concentration of the running buffer should lead to noticeable improvement in resolution (Fig. 13). In fact, the use of low ionic strength buffer should reduce counterion screening,

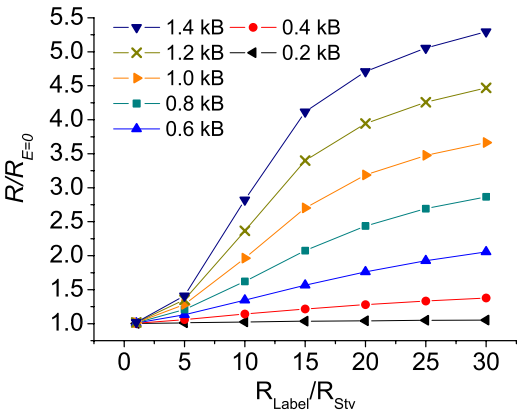

FIG. 10. (Color online) Plots of end-to-end distance R (normalized by equilibrium end-to-end distance at $E=0$) against label radius [normalized by streptavidin radius (2.7 nm)] for a series of DNA sizes.

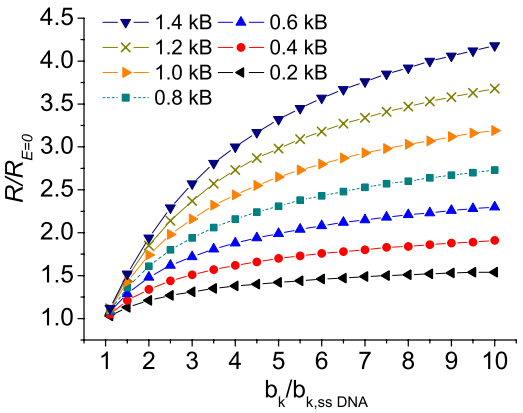

FIG. 12. (Color online) Plots of end-to-end distance R (normalized by equilibrium end-to-end distance at $E=0$) against Kuhn length [normalized by Kuhn length of ssDNA (7 nm)] for different DNA sizes.

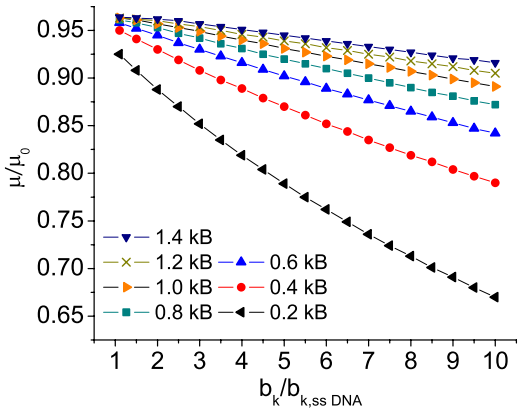

FIG. 13. (Color online) Plots of reduced mobility against Kuhn length [normalized by Kuhn length of ssDNA (7 nm)] for various DNA sizes.

thus enhancing throughput by increasing the mobility of all conjugates.

IV. CONCLUSION

We have studied electrophoresis of hydrodynamically segregated protein-DNA conjugates in free solution. Using an elastic dumbbell model, we show that it is possible to estimate the average end-to-end distance of the labeled DNA during electrophoresis and to compute mobility of the conjugate as a function of applied field, tag size, DNA size, and local stiffness/Kuhn length. A key feature of this model is that field-induced elongation of the DNA fragment intensifies the size-dependence of mobility, which itself has a nonmonotonic dependence on the applied field. One consequence of this interplay is that the size of the label/tag sets the mobility of the conjugate both directly through its surface area and indirectly via its effects on the conformation of the DNA. Indeed, at both low and moderate electric fields, where data is available, we find that the DNA-size dependence of the calculated electrophoretic mobility values are in good to excellent accord with experimental observations for dsDNA labeled with streptavidin. The use of low ionic running buffer is therefore expected to enhance resolution by promoting extended DNA conformations.

ACKNOWLEDGMENTS

This work was supported by the Department of Energy Basic Energy Sciences Program (Grant No. DE-FG02-07ER46455) and by the National Science Foundation Polymers program (Grant No. DMR0551185). Moonsoo Jin is acknowledged for useful discussions regarding biotin-streptavidin interactions and Donald Koch for assistance with model development.

[1] N. C. Stellwagen, C. Gelfi, and P. G. Righetti, Biopolymers **42**, 687 (1997).
[2] P. D. Grossman and J. C. Colburn, *Capillary Electrophoresis: Theory and Practice* (Academic Press, San Diego, 1992).
[3] E. Stellwagen, Y. Lu, and N. C. Stellwagen, Biochemistry **42**, 11745 (2003).
[4] P. Mayer, G. W. Slater, and G. Drouin, Anal. Chem. **66**, 1777 (1994).
[5] D. Long, J.-L. Viovy, and A. Ajdari, J. Phys.: Condens. Matter **8**, 9471 (1996).
[6] D. Long, A. V. Dobrynin, M. Rubinstein, and A. Ajdari, J. Chem. Phys. **108**, 1234 (1998).
[7] C. Desruisseaux, D. Long, G. Drouin, and G. W. Slater, Macromolecules **34**, 44 (2001).
[8] D. Long and A. Ajdari, Electrophoresis **17**, 1161 (1996).
[9] R. J. Meagher, J. I. Won, L. C. McCormick, S. Nedelcu, M. M. Bertrand, J. L. Bertram, G. Drouin, A. E. Barron, and G. W. Slater, Electrophoresis **26**, 331 (2005).
[10] S. Nedelcu, R. J. Meagher, A. E. Barron, and G. W. Slater, J. Chem. Phys. **126**, 175104 (2007).
[11] L. C. McCormick and G. W. Slater, Electrophoresis **28**, 674 (2007).
[12] C. Heller, G. W. Slater, P. Mayer, N. Dovichi, D. Pinto, J. L. Viovy, and G. Drouin, J. Chromatogr. A **806**, 113 (1998).
[13] W. A. Hendrickson, A. Pahler, J. L. Smith, Y. Satow, E. A. Merritt, and R. P. Phizackerley, Proc. Natl. Acad. Sci. U.S.A. **86**, 2190 (1989).
[14] L. C. McCormick and G. W. Slater, Electrophoresis **28**, 3837 (2007).
[15] T. Sano, M. W. Pandori, X. Chen, C. L. Smith, and C. R. Cantor, J. Biol. Chem. **270**, 28204 (1995).
[16] B. A. Williams and G. Vigh, Anal. Chem. **68**, 1174 (1996).
[17] R. B. Bird, O. Hassager, R. C. Armstrong, and C. F. Curtiss, *Dynamics of Polymeric Liquids*, 2nd ed. (Wiley, New York, 1987), Vol. 2: Kinetic Theory.
[18] J. F. Marko and E. D. Siggia, Science **265**, 1599 (1994); Macromolecules **28**, 8759 (1995).
[19] M. Rubinstein and R. Colby, *Polymer Physics* (Oxford University Press, New York, 2004).
[20] S. T. Grosser, J. M. Savard, and J. W. Schneider, Anal. Chem. **79**, 9513 (2007).
[21] J. M. Savard, S. T. Grosser, and J. W. Schneider, Electrophoresis **29**, 2779 (2008).
[22] B. Tinland, A. Pluen, J. Sturm, and G. Weill, Macromolecules **30**, 5763 (1997).